

The influence of superimposed DC current on electrical and spectroscopic characteristics of HiPIMS discharge

Xiao Zuo, Rende Chen, Jingzhou Liu, Peiling Ke, and Aiying Wang

Citation: *AIP Advances* **8**, 015132 (2018);

View online: <https://doi.org/10.1063/1.5018037>

View Table of Contents: <http://aip.scitation.org/toc/adv/8/1>

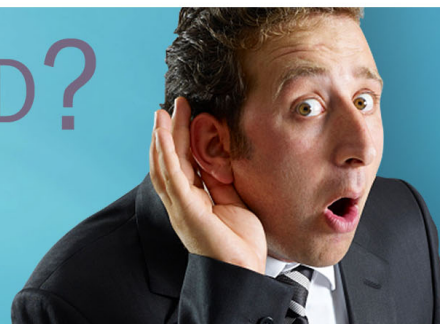
Published by the [American Institute of Physics](#)

HAVE YOU HEARD?

Employers hiring scientists and
engineers trust

PHYSICS TODAY | JOBS

www.physicstoday.org/jobs



The influence of superimposed DC current on electrical and spectroscopic characteristics of HiPIMS discharge

Xiao Zuo,¹ Rende Chen,^{1,2} Jingzhou Liu,^{1,3} Peiling Ke,^{1,a} and Aiyang Wang^{1,a}

¹Key Laboratory of Marine Materials and Related Technologies, Zhejiang Key Laboratory of Marine Materials and Protective Technologies, Ningbo Institute of Materials Technology and Engineering, Chinese Academy of Sciences, Ningbo 315201, China

²University of Chinese Academy of Sciences, Beijing 100049, China

³School of Materials Science and Engineering, Shanghai University, Shanghai 200444, China

(Received 2 December 2017; accepted 22 January 2018; published online 29 January 2018)

The electrical characteristics and spectroscopic properties have been comprehensively investigated in a DC superimposed high power impulse magnetron sputtering (DC-HiPIMS) deposition system in this paper. The influence of superimposed DC current on the variation of target and substrate current waveforms, active species and electron temperatures with pulse voltages are focused. The peak target currents in DC-HiPIMS are lower than in HiPIMS. The time scales of the two main discharge processes like ionization and gas rarefaction in DC-HiPIMS are analyzed. When the pulse voltage is higher than 600 V, the gas rarefaction effect becomes apparent. Overall, the ionization process is found to be dominant in the initial $\sim 100 \mu\text{s}$ during each pulse. The active species of Ar and Cr in DC-HiPIMS are higher than in HiPIMS unless that the pulse voltage reaches 900 V. However, the ionization degree in HiPIMS exceeds that in DC-HiPIMS at around 600 V. The electron temperature calculated by modified Boltzmann plot method based on corona model has a precipitous increase from 0.87 to 25.0 eV in HiPIMS, but varies mildly after the introduction of the superimposed DC current. Additionally, the current from plasma flowing to the substrate is improved when a DC current is superimposed with HiPIMS. © 2018 Author(s). All article content, except where otherwise noted, is licensed under a Creative Commons Attribution (CC BY) license (<http://creativecommons.org/licenses/by/4.0/>). <https://doi.org/10.1063/1.5018037>

I. INTRODUCTION

Microstructure control is of critical importance in the fabrication of hard yet tough as well as dense nanocomposite coatings,^{1–3} which are potentially able to satisfy the harsh wear and corrosion resistant demands in marine applications.^{4,5} According to the extended structure zone diagram proposed by A. Anders,⁶ energetic deposition with large ion fluxes facilitates the control of coating microstructure in plasma based depositions. Very recently, the HiPIMS which features in high ionization degree attracts many attentions for the fabrication of dense and fine crystalline nanocomposite coatings. Besides, the formation of micro-particles can also be eliminated. However, ion transport efficiency from target to substrate is low because of the return of target material ions.⁷ Moreover, reactive HiPIMS suffers frequent arcing due to the non-conductive layer formed on target surface during the afterglow stage. Various methods have been attempted to improve deposition rate and discharge stability, such as magnetic field configuration, hybrid secondary plasma source, and pulse waveform modulation.

D. Lundin *et al.* reported that the cross field ion transport led to deposition rate loss in the direction facing target.⁸ This provides theoretical instruction for the improvement of the target to substrate ion transport efficiency. Decreasing the magnetic field magnitude is an effective way to optimize HiPIMS deposition rate.^{9,10} While, X. B. Tian,^{11,12} P. Raman¹³ and R. Ganesan¹⁴

^aElectronic mail: kepl@nimte.ac.cn and aywang@nimte.ac.cn

recur to external electrical/magnetic field or more efficient magnet distribution. Another commonly utilized approach is hybrid technology, such as hybrid dual-HiPIMS systems,¹⁵ RF (radio frequency)/HiPIMS¹⁶ and DCMS (direct current magnetron sputtering)/HiPIMS co-sputtering processes.¹⁷ Except these traditional DC/mid-/radio-frequency magnetron sputtering sources, secondary plasmas like inductively coupled plasmas (ICPs)¹⁸ and electron cyclotron wave resonance (ECWR) plasmas¹⁹ have also been applied to assist HiPIMS deposition. These hybrid sources cause pre-ionization effect which introduces some important features, including the reduction of working pressure, modulation of ion energy, and increase of deposition rate. Especially, the modulation of ion energy is important for the deposition of nanocomposite coatings. According to Y. T. Pei's work, a broadened ion energy distribution (IED) will result in dense non-columnar structure.^{20,21} However, pulse waveform modulation would be better because no additional auxiliary device is needed, and broadened IED plasma can be obtained in specific area. There are two typical pulse waveform modulation methods including modulated pulse power magnetron sputtering (MPPMS)²² and DC-HiPIMS.

DC current has been applied widely in pulse discharges for pre-ionization to stabilize discharge, and provide seed electrons to reduce working pressure. When Kouznetsov²³ and Helmersson²⁴ reported this new ionized deposition method, HiPIMS was a kind of pulse discharge without superimposed DC current. P. Vašina *et al.* superimposed a pre-ionization low current (about 4 mA) DC discharge with HiPIMS, realized fast and perfectly reproducible discharge.²⁵ In the past several years, this kind of method was adopted to fabricate graphite-like carbon films,^{26,27} MoS₂-C²⁸ and MoS₂-Ti²⁹ composites, TiN coatings,³⁰ where the superior mechanical and tribological performances were discussed in terms of structure. Therefore the superimposed DC current not only optimizes pulse glowing and plasma stabilization through pre-ionization, but also ensures high deposition rate. However, the role of DC current on the performance of HiPIMS discharge has not been clarified clearly. Actually, in the applications of DC-HiPIMS system, the increase of DC current plays key role in both pre-ionization process and film structures.²⁹ In this paper, we focus the effects of superimposed DC current on HiPIMS discharge behaviors from target and substrate current waveforms characterization. In particular, the influence of direct current on the active species in HiPIMS plasma under various pulse voltage conditions are clarified. Target current behaviors and discharge processes under the influence from superimposed DC current are also discussed through the electrical characteristics measurements. Additionally, substrate current behaviors in DC-HiPIMS at different pulse voltage and substrate bias conditions are investigated.

II. EXPERIMENTAL SETUP

Fig. 1 is a schematic diagram of the custom built DC-HiPIMS equipment. The vacuum chamber with the size of 60 cm inner diameter and 60 cm inner height was cryogenically pumped to a base pressure of 3.3×10^{-6} Torr. The pumping speed was controlled via a variable gate valve (VAT). The sputtering gas was Ar with an adjustable flow rate up to 100 sccm by a calibrated mass flow controller (MKS). The base pressure was measured with an ion gauge, while the process pressure was monitored with a capacitance manometer (MKS Baraton). Working pressure was controlled at 3.8 mTorr by the VAT. The rectangular magnetron was fitted with a 40 cm \times 10 cm \times 0.7 cm Cr target. It was supplied by a high power pulse unit (HPPMS-20k, PTL) operating in unipolar constant voltage mode and constant DC current mode. Repetition frequency of the voltage pulse was kept at 50 Hz. A 350 kHz pulsed bias (Pinnacle Plus, Advanced Energy) was applied on substrate holder. The target current was monitored by using a combined current transformer (LEM LT58-S7). The data were recorded with a digital storage oscilloscope (Tektronix TDS 1012C-SC). The optical emission spectra (OES) were acquired *via* the optical fiber and analyzed by Acton Spectra Pro SP-2500 spectrometer (Princeton Instruments) equipped with a grating of 1200 g/mm and a 10 μ m wide slit. This spectrometer was calibrated by typical mercury pen lamps. The collimated optical fiber port was installed parallel to the magnetron with a distance of around 12 cm (as shown in Fig. 1). The integral time and high voltage was set as 1000 ms and 815 V, respectively. When the Single Point Scan mode was selected, typical atomic spectrum lines of Ar and Cr were observed. Four typical spectrum

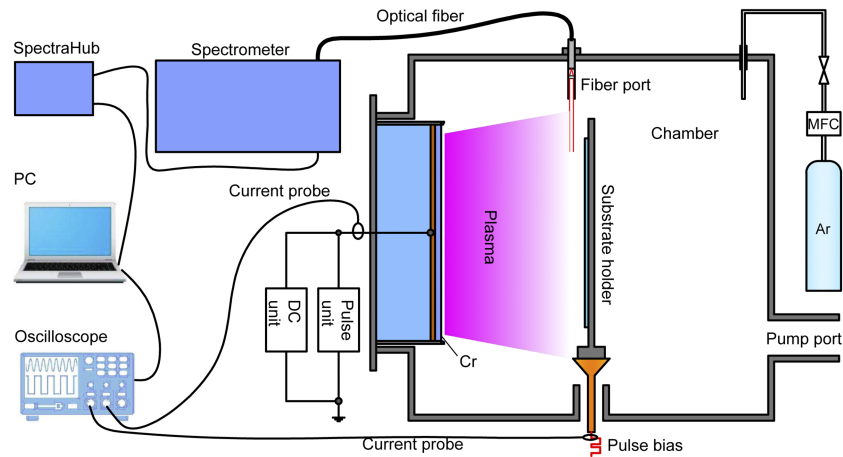


FIG. 1. A schematic diagram of HiPIMS equipment and characterization arrangements.

lines such as Ar^+ (427.9 nm), Ar^* (810.6 nm), Cr^+ (283.6 nm) and Cr^* (359.5 nm) were selected to discuss the plasma properties in DC-HiPIMS discharge processes. In order to reduce errors in the plasma parameters, several independent experiments were performed under the same conditions and the results represented the average of five independent experiments. In addition, pulse voltage is the set output voltage of the power supply, voltage measured on target by oscilloscope is labeled as target voltage.

III. RESULTS AND DISCUSSIONS

A. The influence of superimposed DC current on target current waveforms

The typical HiPIMS target voltage and current waveforms can be found in Ref. 31. When the target voltage is high enough to ionize the Ar gas, voltage breakdown and discharge occurs. After breakdown, the voltage promptly drops to a constant value during the pulse-on stage. For HiPIMS and DC-HiPIMS processes, the target current waveforms under various pulse voltage conditions are shown in Fig. 2. The pulse width is 200 μs , no self-sustained self-sputtering is observed. The rising of target current in HiPIMS has apparent delay to target voltage pulse. With the increase of pulse voltage, it reduces to about 14 μs at 600 V, and holds on a nearly constant value when pulse voltage is between 600 and 950 V. G. Y. Yushkov *et al.* attributes this phenomenon to the time needed for ionization avalanches to grow and ionization cycles to complete.³² When a 1.0 A DC current is superimposed with HiPIMS, the delay of rising current and the vibration of target current are eliminated. However, the transient target current is weakened after the introduction of the DC current. Besides, it also has

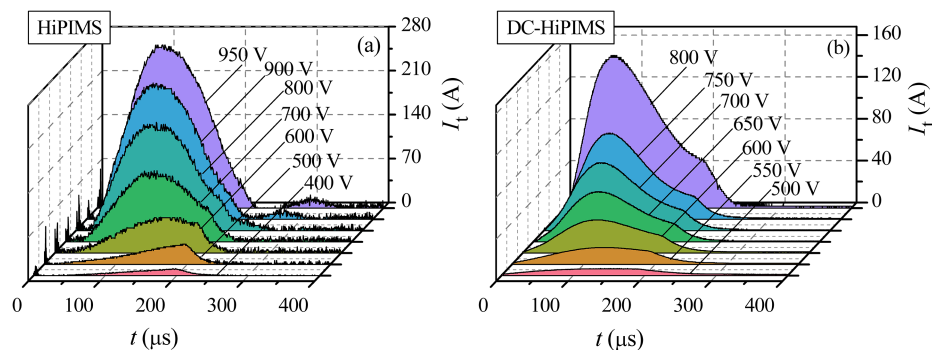


FIG. 2. Target current waveforms at various pulse voltages for (a) HiPIMS and (b) DC-HiPIMS.

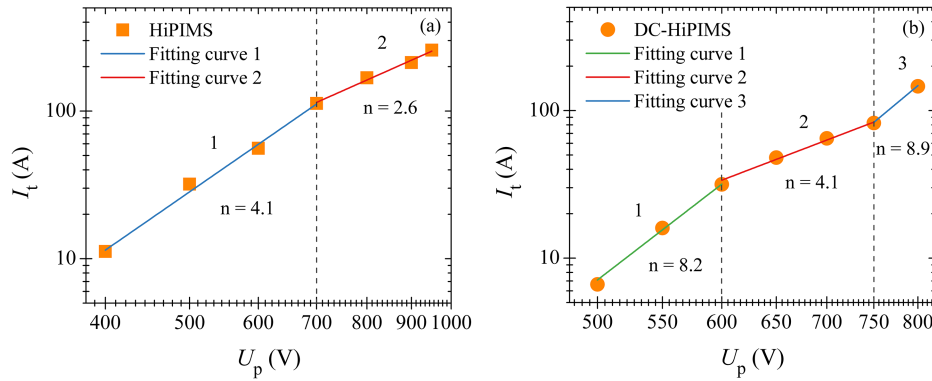


FIG. 3. The variation of peak target current with pulse voltages for (a) HiPIMS and (b) DC-HiPIMS.

impacts on the behaviors of target current waveform. Peak target current and its corresponding time for each pulse voltage are presented in Fig. 3 and Fig. 4, respectively.

According to the relationship between peak target current and pulse voltage reported by J. Alami,³³ it follows a power law as formula (1).

$$I_{pt} = kU_p^n \quad (1)$$

where, I_{pt} and U_p are peak target current and pulse voltage respectively, k is a constant value. For conventional DCMS, n ranges between $5 < n < 15$. In Fig. 3 it is found that n for DC-HiPIMS is higher than HiPIMS. Additionally, it is as expected that the variation of target current with pulse voltage shows stage features. In DC-HiPIMS n varies among 8.2, 4.1 and 8.9 with the increase of pulse voltage. However, in HiPIMS n reduces from 4.1 to 2.6 when pulse voltage is higher than 700 V. The reduction of n is attributed to gas rarefaction effect under high discharge power conditions. The decrease of gas density near target region leads to an increase in plasma impedance. The higher n values in DC-HiPIMS indicates that the discharge is DCMS-like with low plasma impedance. Thus, although peak target current of DC-HiPIMS is lower than HiPIMS, its difference between them is reduced at high pulse voltages. Since the target current is composed of incident ion current and secondary electron current emitted from target surface under the bombardment of ions, a reduction in peak target current indicated lowered ion density during the pulse-on stage in DC-HiPIMS.

Except the decreased peak target current compared to HiPIMS, the peak target current time (τ_{cp}) in DC-HiPIMS is also reduced, which is shown in Fig. 4. It is around 150 μs at 500 V, about 40 μs earlier than the 190 μs of HiPIMS. No matter with the change of pulse voltage, target currents in DC-HiPIMS reach maximums faster than that in HiPIMS. For HiPIMS discharge, when the pulse

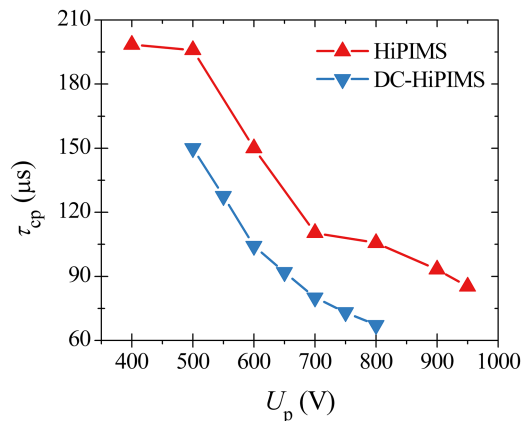


FIG. 4. The variation of peak current time with pulse voltages for HiPIMS and DC-HiPIMS.

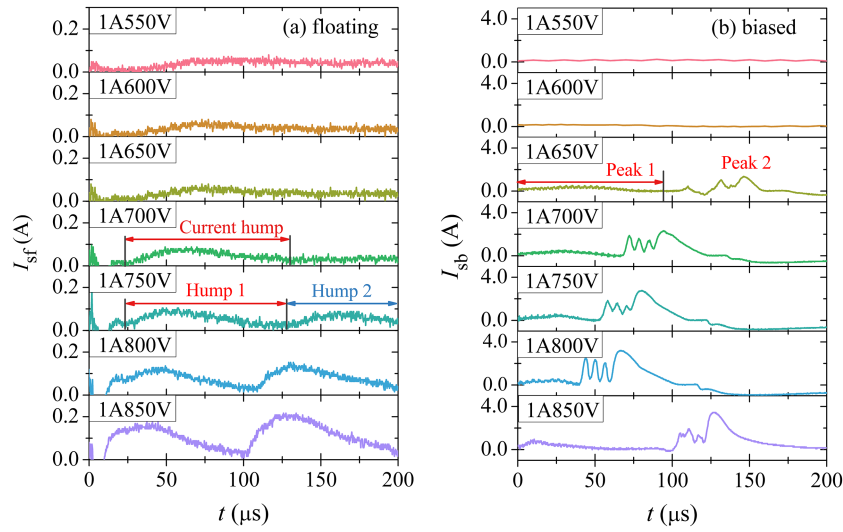


FIG. 5. The variation of substrate current with pulse voltage at (a) floating and (b) -50 V.

voltage is below 500 V (Fig. 2a), gas rarefaction isn't observed in the target current waveforms, where the maximum current time is around 200 μs (Fig. 4). From 500 V to 700 V, it decreases from 200 μs to 110.4 μs . Further the increase of pulse voltage to 950 V leads to the decrease of it to 85.2 μs . This tendency is consistent with the variation behaviors of target current waveforms. When pulse voltage is higher than 600 V, target currents decrease after their maximums. This feature could be attributed to the obvious gas rarefaction effect at high pulse voltage conditions, since more power could be coupled into plasma. Once gas rarefaction happens, fewer Ar^+ would be attracted to the target, which results in the decrease of target current. The time corresponding to peak target current reflects the competitive processes between ionization and gas rarefaction. It will be discussed in the following section.

B. The electrical characteristics of substrate current waveforms

The temporal evolution of target current indicates that plasma varies with time in HiPIMS/DC-HiPIMS. Since the plasma is transient, its influence on the substrate current is crucial in film deposition process. The substrate current composes of ion current and electron current between plasma and the substrate. In this part, the temporal evolutions of substrate currents under different pulse voltage conditions are investigated. Fig. 5 illustrates the substrate current waveforms in DC-HiPIMS. Fig. 5a shows the substrate current waveforms at different pulse voltages when substrate is electrically floated. The substrate currents with pulse voltage at 550 V and 600 V fluctuate around 0.064 A. However, the currents show an about 100 μs width hump for each at 650 V and 700 V. Further increase in the pulse voltage results in a second hump. Meanwhile, the second current peak becomes stronger than the first peak. The details of the substrate current waveforms are list in Table I, where, t_{rs} is rising time of the second peak, I_{p1} and I_{p2} are first and second peak values of the substrate current waveforms. It is

TABLE I. The substrate current maximums and rising time of the second current peak.

U_p (V)	t_{rs} (μs)	I_{p1} (A)	I_{p2} (A)	I_{p2}/I_{p1}
550	--	0.064	--	--
600	149.4	0.064	--	--
650	146.2	0.064	--	--
700	127.8	0.088	--	--
750	119.2	0.104	0.088	0.85
800	103.0	0.136	0.136	1.0
850	100.2	0.176	0.216	1.23

obvious that the width of the first hump is not equal to the target pulse width. It reduces to 100.2 μs when the pulse voltage is 850 V. The rising time of the second hump is comparable to the time of peak target current in Fig. 2. As the substrate is set as floating, the ion current and the electron current should vary to reach a dynamic equilibrium. The variation of substrate currents reflects the temporal evolution of HiPIMS plasma. Thus, the competitive processes between ionization and gas rarefaction could be qualitatively analyzed at various pulse voltages by discussing substrate current waveforms.

The ionization and gas rarefaction are in opposite positions for the variation of plasma in DC-HiPIMS. As shown in Fig. 2 and 4 when the pulse voltage is low, ionization is the dominant process. Plasma density in this process will continuously increase during pulse-on stage. With the increase of pulse voltage, not only the ionization is enhanced, but also the gas rarefaction effect is. After breakdown, gas rarefaction effect is weak, the ionization process leads to the rapid increase of plasma density. When the substrate current reaches the first peak, the variation of plasma density becomes small. In Fig. 5a the accumulated heat results in gas rarefaction at around 50 μs , which suppresses the rapid increase of plasma density. With the increased influence from the gas rarefaction, the plasma density reached to a maximum. After that the gas rarefaction becomes so strong that the plasma density starts to decrease. From the increase of the second hump in the substrate current, plasma density presents a rapid decrease. However, after the second peak in the substrate current at around 150 μs , the decrease of plasma density slows down. This can be explained as that gas rarefaction lowers the density of Ar atoms, which improves the mean free path of the electrons, and the ionization process with more energized electrons. Therefore, the decrease of plasma density slows down.

Fig. 5b demonstrates the substrate current waveforms when a -50 voltage bias is applied on the substrate holder. The substrate currents keep nearly constant during the pulse at 550 and 600 V. When pulse voltage reaches to 650 V, two main peaks appeared in the substrate current waveforms. The first one is below 1.0 A, the second one could reach to about 4.0 A. With the increase of pulse voltage, the first one increases and the second one seems to reach a stable value. The width of the first peak becomes more and more narrow. As a result the current peaks all appear in 100 μs . This result suggests a reduced pulse width around 100 μs for DC-HiPIMS discharge.

C. Analysis of optical emission spectroscopic measurements

The influence of different DC currents, like 0.5, 1.0, 2.0, 3.0 and 4.0 A, on HiPIMS plasmas properties has been investigated with pulse voltage at 700 V. It is found that with the increase of DC current the spectral line intensities of Ar^+ , Ar^* and Cr^* are all improved, but the intensity of Cr^+ is reduced. Considering the low and reduced Cr^+ line intensity ratio, it is suggested that DC current should not exceed 1.0 A. Therefore, the superimposed DC current in this paper is set as 1.0 A with the power of 443 W. The results from OES measurements are presented in Fig. 6. The variation of typical spectral line intensities of Ar^+ and Ar^* (Ar II 427.9 nm and Ar I 810.6 nm), Cr^+ and Cr^* (Cr II 283.6 nm and Cr I 359.5 nm) are plotted in Fig. 6a and 6b, respectively. Fig. 6c and 6d shows the spectral line intensity ratio of Ar^+ (α_{Ar^+}) and Cr^+ (α_{Cr^+}) respectively, which are defined in the following equations:

$$\alpha_{\text{Ar}^+} = \frac{I_{\text{Ar}^+}}{I_{\text{Ar}^+} + I_{\text{Ar}^*}} \quad (2)$$

$$\alpha_{\text{Cr}^+} = \frac{I_{\text{Cr}^+}}{I_{\text{Cr}^+} + I_{\text{Cr}^*}} \quad (3)$$

Where, I_{Ar^+} , I_{Ar^*} , I_{Cr^+} and I_{Cr^*} are the intensities of the four Ar and Cr atomic spectral lines.

The intensity of Ar^* line in DC-HiPIMS is determined by DCMS since it nearly keeps constant regardless of the variation of pulse voltage. It is several times stronger than the Ar^* line intensity in HiPIMS, indicating that more metastable Ar atoms exist in DC-HiPIMS. The intensity of Ar^+ line increases with pulse voltage in both HiPIMS and DC-HiPIMS conditions. Initially, the Ar^+ line intensity in DC-HiPIMS is higher than in HiPIMS. But the difference between each other became smaller with the increase of pulse voltage. They reach the same value at 900 V. Taking considering of Ar^+ line intensity ratio, in HiPIMS it is weaker than that in DCMS with $U_p < 600$ V. The variation trend of Cr^* line intensity with pulse voltage is similar to the Ar^+ line intensity. It can be understood

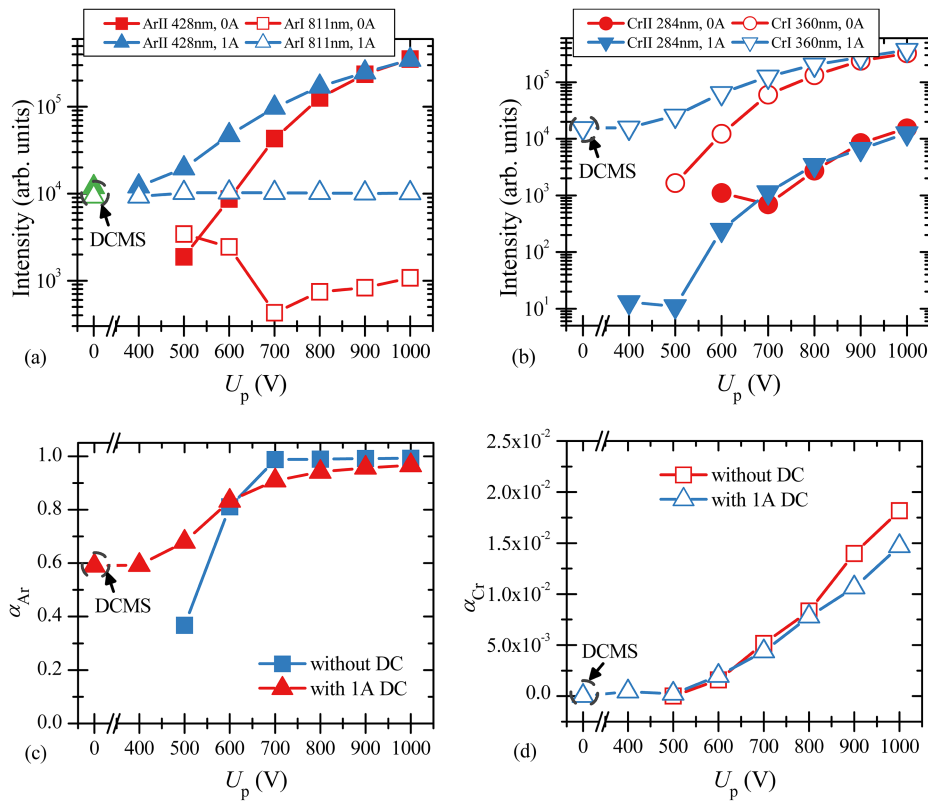


FIG. 6. The variation of typical Ar and Cr spectral line intensities and ratios with pulse voltages.

that since Cr atoms are sputtered from target under the bombardment of Ar^+ with incident ion energy dependent sputtering yield. Note that although the intensity of Cr^+ line in both HiPIMS and DC-HiPIMS are much stronger than that in DCMS, it is far weaker than Cr^* line intensity. When the pulse voltage is higher than 700 V, the Cr^+ line intensity in HiPIMS and DC-HiPIMS are nearly equivalent as shown in Fig. 7.

The ratio of Ar^+ line intensity is about 0.6 in DCMS. It increases with pulse voltage in both HiPIMS and DC-HiPIMS processes. However, when pulse voltage is below 550 V in HiPIMS, it is less than 0.4. As the pulse voltage increases to 600 V, The ratio of Ar^+ line intensity in HiPIMS is equivalent to that in DC-HiPIMS. At last it exceeds the ratio of Ar^+ line intensity in DC-HiPIMS when pulse voltage is 700 V, and reaches a stable value around 0.99. Meanwhile, when pulse voltage is higher than 500 V, the ratio of Cr^+ line intensities in HiPIMS and DC-HiPIMS are higher than DCMS. However, when pulse voltage is higher than 800 V, the ratio of Cr^+ line intensity in HiPIMS becomes higher than DC-HiPIMS. Therefore, the superimposed DC current at high pulse voltage conditions (above 700 V) would limit the increase of ion density or ionization degree.

HiPIMS discharge generates non-equilibrium plasma with the temperature of electrons higher than the neutral gas temperature. Plasma in HiPIMS/DC-HiPIMS are far from localized temperature equilibrium (LTE) plasma, we apply the corona model and use a modified Boltzmann formula as follows to determine the excitation temperature, which can give a first estimation of the electron temperature.^{34,35}

$$\ln \left(\frac{I_{ij} \lambda_{ij} \sum_{i>j} A_{ij}}{A_{ij} a_{1i}} \right) = -\frac{E_i}{k_B T_e} + \text{const.} \quad (4)$$

where I_{ij} and λ_{ij} are, respectively, the intensity and wavelength of spectral lines, A_{ij} is the Einstein coefficient, E_i is the excitation energy of level i , k_B is the Boltzmann constant, and a_{1i} is the coefficient in an exponential approximation of the electron-impact excitation rate coefficient from ground state to level i . Fig. 8 shows the modified Boltzmann plot obtained from Ar lines for 1.0 A DCMS. The electron temperatures found by linear fitting of the Ar peaks (687.1, 696.5, 706.8, 714.7, 750.4, 764.1 and

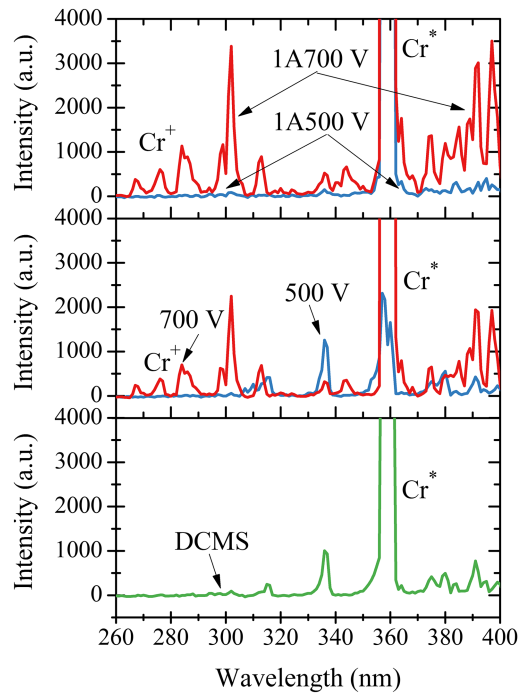


FIG. 7. OES spectra of DCMS, HiPIMS and DC-HiPIMS sputtering of Cr in Ar atmosphere.

810.6 nm) for DCMS, HiPIMS and DC-HiPIMS are plotted in Fig. 9. Electron temperature in 1.0 A DCMS plasma is around 0.55 eV. The values of electron temperature in HiPIMS and DC-HiPIMS plasma measured by OES with pulse voltage below 600 V are varied around the electron temperature of 1.0 A DCMS. However, the electron temperature in HiPIMS presents rapid increase to about 25.0 eV from 600 to 800 V. Therefore, the rapid increase of peak target current and the decrease of the corresponding time can be understood.

D. The influence of superimposed DC current on substrate current waveforms

The substrate current waveforms of HiPIMS and DC-HiPIMS under various bias conditions at 700 V are demonstrated in Fig. 10. The measured substrate currents have kHz pulses within the 50 Hz pulse envelope curve. Overall, high bias voltage leads to an apparent increase of substrate current. In Fig. 10a, as the substrate bias is increased to -200 V, there are two apparent humps in the current waveforms. The current maximum reaches 10.8 A at -250 V. The first hump width is around

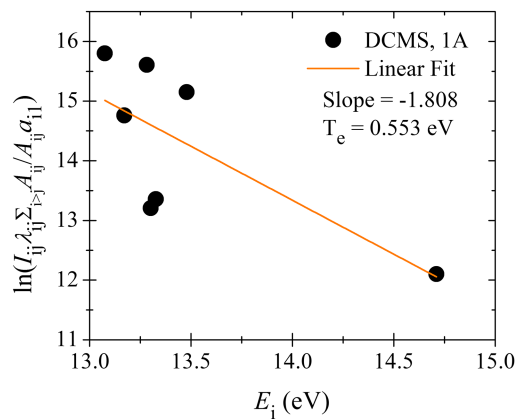


FIG. 8. The modified Boltzmann plot obtained from Ar lines for 1.0 A DCMS.

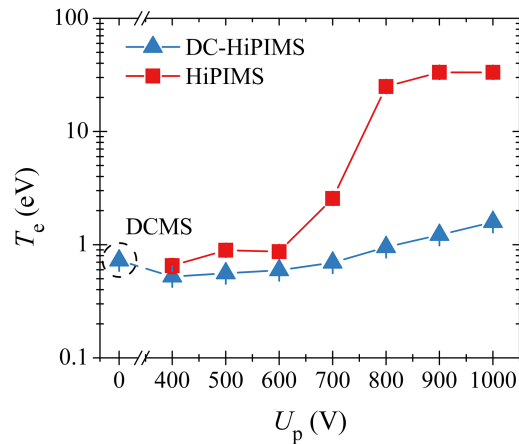


FIG. 9. Comparison of electron temperatures as a function of pulse voltage in HiPIMS and DC-HiPIMS.

100 μ s. However, the second hump width and position are changed with the bias from -200 V to -250 V, but all disappeared at 250 μ s. Fig. 10b shows the substrate current waveforms of DC-HiPIMS discharge. It can be found that not only the current maximum decreases, but also the width of current hump lengthens. The fluctuations caused by HiPIMS are depressed by the DCMS plasma. The ion flux and ion energy to the substrate are the two key impactors in coatings preparation of magnetron sputtering processes. Therefore, the ion flux is improved in DC-HiPIMS compared with HiPIMS.

The plasma density in magnetron sputtering decays along the distance from the target to the substrate. The variation of plasma density near target surface at low pulse voltage can't be fully reflected in substrate current waveforms (Fig. 5). But when the pulse voltage is higher than 700 V, the second hump in substrate current waveforms has been detected. Meanwhile the current humps can be detected at higher substrate biases (Fig. 10). The width of the first hump is not equal to the 200 μ s pulse width. But it consists with the time length of ionization stage in target current waveforms, where the gas sputtering is dominant. Then the discharge steps into another stage where gas assisted self-sputtering would be dominant due to the gas rarefaction effect. Therefore, the gas ions flux contributes to the first hump in substrate current waveforms.

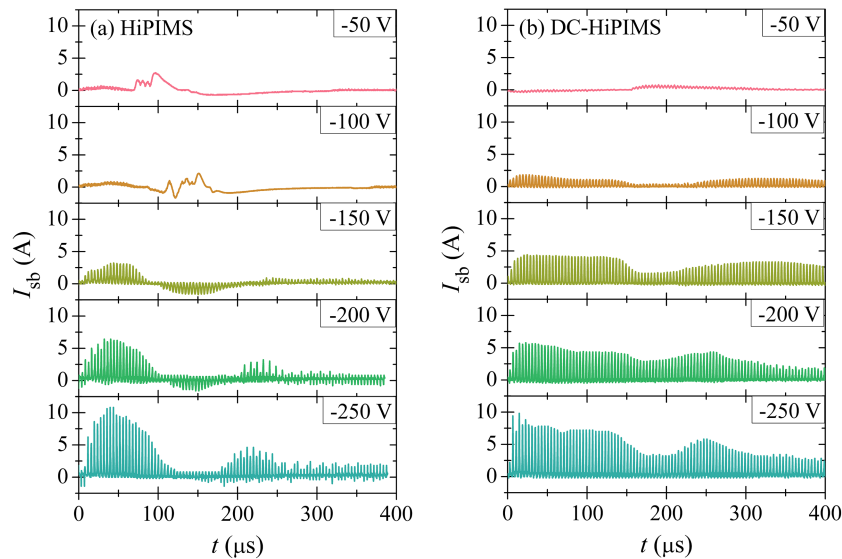


FIG. 10. The influence of DC current on the substrate current waveforms at various bias voltages: (a) HiPIMS and (b) DC-HiPIMS.

IV. CONCLUSIONS

The electrical and spectroscopic characteristics of HiPIMS and DC-HiPIMS are comparatively investigated by the oscilloscope and OES measurements. The DC current has great impacts on the discharge in DC-HiPIMS. After the introduction of the superimposed 1.0 A DC current, the peak target currents in DC-HiPIMS are lower than in HiPIMS. They both show stage characteristics with the increase of pulse voltage. The rising rates of target current increase with the improvement of pulse voltage. However, it increases much faster in DC-HiPIMS than in HiPIMS. Furthermore, the competitive relationship between ionization and gas rarefaction has been discussed through the analysis of substrate current waveforms. The ionization process is found to be dominant in the first 100 μ s. OES diagnosis results demonstrate that the contents of Ar⁺ and Cr* at low pulse voltages in DC-HiPIMS are higher than HiPIMS. But the difference becomes small with the increase of pulse voltage. The corona model is utilized to calculate electron temperature in HiPIMS/DC-HiPIMS discharge. When the pulse voltage is higher than 600 V, electron temperature in HiPIMS rapidly increases to more than 25.0 eV, but changes more moderate in DC-HiPIMS. Nevertheless the ionization degree in DC superimposed condition is reduced. Additionally, the temporal evolution of substrate current waveform becomes more consecutive and changes mildly.

ACKNOWLEDGMENTS

This research was supported by the project of the State Key Project of Fundamental Research of China (2017YFB0702303), National Natural Science Foundation of China (11705258, 51522106), Zhejiang Key Research and Development Program (2017C01001), Natural Science Foundation of Ningbo (2017A610012).

- ¹ R. H. Wei, *Surf. Coat. Tech.* **203**(5-7), 538–544 (2008).
- ² Q. M. Wang and K. H. Kim, *Acta Mater.* **57**(17), 4974–4987 (2009).
- ³ S. G. Zhou, L. P. Wang, Z. B. Lu, Q. Ding, S. C. Wang, R. J. K. Wood, and Q. J. Xue, *J. Mater. Chem.* **22**(31), 15782–15792 (2012).
- ⁴ A. Leyland and A. Matthews, *Wear* **246**(1-2), 1–11 (2000).
- ⁵ Z. W. Wu, F. Zhou, Q. Ma, Q. Z. Wang, Z. F. Zhou, and L. K. Y. Li, *RSC Adv.* **6**(80), 76724–76735 (2016).
- ⁶ A. Anders, *Thin Solid Films* **518**(15), 4087–4090 (2010).
- ⁷ T. Kozak and J. Vlcek, *Plasma Sources Sci. T.* **22**(1), 015009 (2013).
- ⁸ D. Lundin, P. Larsson, E. Wallin, M. Lattemann, N. Brenning, and U. Helmersson, *Plasma Sources Sci. T.* **17**(3), 035021 (2008).
- ⁹ J. Capek, M. Hala, O. Zabeida, J. E. Klemberg-Sapieha, and L. Martinu, *J. Phys. D: Appl. Phys.* **46**(20), 205203 (2013).
- ¹⁰ J. W. Bradley, A. Mishra, and P. J. Kelly, *J. Phys. D: Appl. Phys.* **48**(21), 215202 (2015).
- ¹¹ X. B. Tian, Y. H. Ma, J. Hu, M. K. Bi, C. Z. Gong, and P. K. Chu, *J. Vac. Sci. Technol. A* **35**(2), 021402 (2017).
- ¹² C. W. Li and X. B. Tian, *Rev. Sci. Instrum.* **87**(8), 083507 (2016).
- ¹³ P. Raman, I. Shchelkanov, J. McLain, M. Cheng, D. Ruzic, I. Haehnlein, B. Jurczyk, R. Stubbers, and S. Armstrong, *Surf. Coat. Tech.* **293**, 10–15 (2016).
- ¹⁴ R. Ganesan, B. Treverrow, P. Denniss, D. G. McCulloch, D. R. McKenzie, and M. M. M. Bilek, *J. Appl. Phys.* **120**(10), 103301 (2016).
- ¹⁵ V. Stranak, S. Drache, R. Bogdanowicz, H. Wulff, A. P. Herrendorf, Z. Hubicka, M. Cada, M. Tichy, and R. Hippler, *Surf. Coat. Tech.* **206**(11-12), 2801–2809 (2012).
- ¹⁶ N. Holtzer, O. Antonin, T. Minea, S. Mamieros, and D. Bouchier, *Surf. Coat. Tech.* **250**, 32–36 (2014).
- ¹⁷ K. Bobzin, T. Brogelmann, N. C. Kruppe, and M. Engels, *Thin Solid Films* **620**, 188–196 (2016).
- ¹⁸ H. T. Zhang, J. Y. Chen, J. Cherng, Z. D. Wang, Z. W. Liu, and Q. Chen, *J. Cryst. Growth* **453**, 138–142 (2016).
- ¹⁹ V. Stranak, A. P. Herrendorf, S. Drache, M. Cada, Z. Hubicka, M. Tichy, and R. Hippler, *Appl. Phys. Lett.* **100**(14), 141604 (2012).
- ²⁰ C. Q. Chen, Y. T. Pei, K. P. Shaha, and J. T. M. De Hosson, *Appl. Phys. Lett.* **96**(7), 073103 (2010).
- ²¹ Y. T. Pei, A. A. Turkin, C. Q. Chen, K. P. Shaha, D. Vainshtein, and J. T. M. De Hosson, *Appl. Phys. Lett.* **96**(15), 151910 (2010).
- ²² J. Lin, J. J. Moore, W. D. Sproul, B. Mishra, J. A. Rees, Z. Wu, R. Chistyakov, and B. Abraham, *Surf. Coat. Tech.* **203**(24), 3676–3685 (2009).
- ²³ V. Kouznetsov, K. Macak, J. M. Schneider, U. Helmersson, and I. Petrov, *Surf. Coat. Tech.* **122**(2-3), 290–293 (1999).
- ²⁴ K. Macak, V. Kouznetsov, J. Schneider, U. Helmersson, and I. Petrov, *J. Vac. Sci. Technol. A* **18**(4), 1533–1537 (2000).
- ²⁵ P. Vasina, M. Mesko, L. de Poucques, J. Bretagne, C. Boisse-Laporte, and M. Touzeau, *Plasma Sources Sci. T.* **17**(3), 035007 (2008).
- ²⁶ X. Q. Zhang, P. L. Ke, A. Y. Wang, M. D. Huang, and K. H. Kim, *T. Nonferr. Metal. Soc.* **22**, S740–S744 (2012).
- ²⁷ M. D. Huang, X. Q. Zhang, P. L. Ke, and A. Y. Wang, *Appl. Surf. Sci.* **283**, 321–326 (2013).
- ²⁸ L. Gu, P. L. Ke, Y. S. Zou, X. W. Li, and A. Y. Wang, *Appl. Surf. Sci.* **331**, 66–71 (2015).
- ²⁹ X. P. Qin, P. L. Ke, A. Y. Wang, and K. H. Kim, *Surf. Coat. Tech.* **228**, 275–281 (2013).

- ³⁰ Z. Y. Wang, D. Zhang, P. L. Ke, X. C. Liu, and A. Y. Wang, *J. Mater. Sci. Technol.* **31**(1), 37–42 (2015).
- ³¹ X. Zuo, P. L. Ke, R. D. Chen, X. W. Li, M. Oden, and A. Y. Wang, *Phys. Plasmas* **24**(8), 030801 (2017).
- ³² G. Y. Yushkov and A. Anders, *IEEE T. Plasma Sci.* **38**(11), 3028–3034 (2010).
- ³³ J. Alami, K. Sarakinos, G. Mark, and M. Wuttig, *Appl. Phys. Lett.* **89**(15), 104104 (2006).
- ³⁴ B. Vandersijde and J. A. M. Vandermullen, *J. Quant. Spectrosc. Ra.* **44**(1), 39–46 (1990).
- ³⁵ M. A. Song, Y. W. Lee, and T. H. Chung, *Phys. Plasmas* **18**(2), 023504 (2011).